Journal of Alloys and Compounds 504 (2010) 585–593

Contents lists available at ScienceDirect

Journal of Alloys and Compounds

journal homepage: www.elsevier.com/locate/jallcom

The microstructure, mechanical and corrosion properties of calcium polyphosphate reinforced ZK60A magnesium alloy composites

Ailing Feng, Yong Han*

State-Key Laboratory for Mechanical Behavior of Materials, Xi'an Jiaotong University, Xi'an 710049, China

ARTICLE INFO

Article history:
Received 31 March 2010
Received in revised form 28 May 2010
Accepted 1 June 2010
Available online 11 June 2010

Keywords:
Magnesium
Composite
Calcium polyphosphate
Strength
Corrosion
Powder metallurgy

ABSTRACT

The calcium polyphosphate (CPP) reinforced ZK60A magnesium-matrix composites are fabricated using powder metallurgy. In this study, the microstructure, mechanical and corrosion properties of the composites are investigated. The CPP particles are uniformly distributed throughout the composite with firmly bounded CPP–matrix interface. The composites consisted of 20 wt.% CPP achieved a maximum compressive strength of 494.88 MPa. Effective load transfer from matrix to particle results in particle fracture observed during compressive tests. Tensile tests show that the ultimate strength and yield strength of the composites were reduced by CPP addition. The fracture surfaces of composites observed during tensile tests show matrix deformation, interfacial detachment and particle breakage coupled with microscopic crack. The composites enhance the corrosion resistance of materials and exhibit a more uniform corrosion attack in immersion tests and electrochemical tests. Furthermore, CPP accelerates the precipitate of hydroxyapatite in the composites. These results suggest that the CPP_p/ZK60A composite is a promising candidate for degradable implant materials.

1. Introduction

There is a huge demand in the implant markets of medical science in the world currently [1]. The traditional metal implants, such as stainless steels, Ti alloys and cobalt–chromium-based alloys may release toxic metallic ions and particles due to corrosion which can lead to physiological inflammatory effects [2,3]. Moreover, the permanent implants can cause stress-shielding effect due to mismatching in Young's modulus between the implant and the body, which obstructs the stabilization of the bone tissues that need mechanical loads to maintain their rigidity, subsequently reduce bone formation. Biodegradable implants can be gradually dissolved, absorbed, consumed or excreted in a biological environment, so there is no need for a secondary surgery to remove implants after the surgery regions have healed. Unfortunately, currently used biodegradable implants, such as polylactic acid (PLA), have unsatisfactory mechanical properties, and therefore their clinical applications are limited.

Magnesium and its alloys offer an intriguing solution to the problems with conventional metals and polymeric materials utilized for orthopedic implants. Magnesium is biodegradable in body fluids owing to corrosion. Magnesium ions present in large amount (the fourth most abundant cations) in the human body and are involved in many metabolic reactions and biological mechanisms which serve as a cofactor for many enzymes [2]. Magnesium ions accumulate in bone as substitution ions in hydroxyapatite crystal, adsorbing ions at the crystal surface and binding with organic substances. The redundant magnesium can be harmlessly excreted through urination. The specific density (1.74–2 g/cm^3) and Young's modulus (41–45 GPa) of magnesium are close to those (1.8–2.1 g/cm^3, 3–20 GPa) of human bone [2]. Magnesium alloys are able to enhance the osteoblastic activity around the degrading implants and finally lead to a complete replacement of the implants by bone tissue [4,5]. Witte et al. [6] have reported that the corrosion layer of the magnesium alloys is in direct contact with the surrounding bone during degradation which results in an accumulation of biological calcium phosphates. Witte et al. [7] have also demonstrated that the fast-degrading open porous scaffolds made of magnesium alloy AZ91D exhibit a late stage of phase II host response to biodegradable materials at 3 months after surgery, which then turn into a fibrous capsule formation during phase III until 6 months. The biodegradable magnesium stents have been manufactured and undertaken clinical trials.

The major drawback of magnesium alloys is that they suffer from a high corrosion rate in the physiological environment with high chloride concentration and a pH value 7.4–7.6, and thereby they lose their mechanical integrity before tissues have fully recovered. Furthermore, the degradation of magnesium alloys always leads to hydrogen evolution and alkalization of the solution. One

* Corresponding author. Tel.: +86 29 82665580; fax: +86 29 82663453.
E-mail address: yonghan@mail.xjtu.edu.cn (Y. Han).

0925-8388/$ – see front matter © 2010 Elsevier B.V. All rights reserved.
doi:10.1016/j.jallcom.2010.06.013

strategy to resolve these problems is to slow down the biodegradation rate of magnesium, so decrease the releasing rate of Mg^{2+}, H_2 and OH^- and allow sufficient time for human body to response to biodegradation products [8]. The biodegradation rate of magnesium can be adjusted in various ways, mainly by alloying, surface treatment and forming magnesium-matrix composites (MMCs). In fact, a few preliminary trials for improving the corrosion resistance of magnesium implants by surface treatment have been reported in the literature, including alkali-heat-treatment [9], hydroxyapatite coating by electrodeposition [10], fluoride coating by conversion treatment [11], plasma immersion ion implantation and deposition [12], and titanium ion implantation [13]. Other effective method to enhance the corrosion resistance of magnesium is to introduce alloy elements. By alloying, Song [8] has indicated that the hydrogen evolution rate of the Mg2Zn0.2Mn alloy slows down. Recently, calcium is also used to adjust the susceptibility of magnesium to corrode because calcium is a major component in human bone and calcium plays an essential role in cell signally pathways [14,15]. The *in vivo* degradation behavior of Mg–Mn–Zn alloy has showed no inflammation and approximately 54% magnesium implant has degraded after 18 weeks post-operation [16].

An alternative way to enhance the corrosion resistance is to form MMCs reinforced with bioactive ceramic. The advantages to use MMC as biomaterial are due to its adjustable mechanical properties (Young's modulus, tensile strength) as well as the adjustable tailored properties, which can be achieved by choosing appropriate matrix and reinforcement. Witte et al. [17] have reported that MMCs utilizing AZ91D magnesium matrix with embedded hydroxyapatite are cytocompatible with adjustable mechanical and corrosive properties. However, the utilization of aluminum in the MMC limited its application, since aluminum contributes to the impairment of phosphorous metabolism which induces dementia and subsequently causes never toxicity [8,14]. Moreover, the remaining hydroxyapatite after matrix degradation may elicit inflammatory response resulting in bone degeneration [18].

Zinc is recognized as a highly essential element for humans. In zinc deficiency, nearly all the physiological functions are strongly perturbed. Zirconium possesses a set of suitable properties for orthopedic applications such as low specific weight, high corrosion resistance, and biocompatibility [19]. Based on the aforementioned considerations, ZK60A magnesium alloy including Zn and a very small amount of Zr was chosen in our studies to improve corrosion resistance and mechanical properties of magnesium. Calcium polyphosphate (CPP) has drawn much attention due to its similar chemical ingredient to bones and its degradability in biological environments [20]. CPP is a member of the condensed phosphate family formed by repeated condensation of tetrahedral $(PO_4)^{3-}$ groups and has a Ca/P ratio of 0.5. There are four forms of CPP; monoclinic β-CPP is stable under room temperature. CPP, while being only slightly soluble in aqueous solution, is susceptible to hydrolytic degradation by scission primarily of the end phosphate groups [21]. The degradation product is calcium orthophosphate, a naturally occurring and readily metabolizable substance. The *in vivo* studies have showed that the porous CPP promote rapid bone ingrowth and can be tailored to degrade at a given rate *in vivo* through the appropriate selection of starting particle size [22]. Thus, due to its good biocompatibility and biodegradation, β-CPP is used as reinforcement in our study.

Table 1
Materials designation.

Sample	wt. (CPP, %)	Designation
ZK60A	0	**A**
$10CPP_p$/ZK60A	10	**C1**
$20CPP_p$/ZK60A	20	**C2**
$30CPP_p$/ZK60A	30	**C3**

In this study, we successfully prepared three kinds of magnesium-matrix composites using magnesium alloy ZK60A matrix with various amount of CPP as reinforcement by powder metallurgy. We have also studied their microstructure, mechanical properties and corrosion properties *in vitro*.

2. Experimental methods

Calcium polyphosphate bulk was prepared in accordance with reference [23]. Subsequently, CPP powder was produced by planetary ball milling using Al_2O_3 ceramic balls and pots in ethanol. The average diameter of CPP powder was less than 10 μm. Atomized ZK60A powders (WeiHao Corporation of China) had a composition of 5.2107 wt.% Zn, 0.34 wt.% Zr and balanced Mg. The size of the ZK60A powders was less than 50 μm. The CPP_p/ZK60A composite was fabricated by conventional powder metallurgy. The weight percent of CPP was 10%, 20% and 30%, respectively. The designation of the samples was listed in Table 1. The details for powder metallurgy processing were described as following. At first, ZK60A powder and CPP powder were mixed in a three-dimensional blending machine with a rotation speed of 30 rpm for 1 h. The mixed powder was then dried at 120 °C in a vacuum oven for 2 h. Then the powder mixture was cold-pressed into cylindrical compact with a diameter of 40 mm at 400 MPa. The compact was hot-pressed at 380 °C with a pressure of 150 MPa for 20 min. Finally, the materials were hot-extruded into rod with a diameter of 10 mm at 380 °C and an extrusion ratio of 16/1. ZK60A magnesium alloy was prepared using the same method for control.

Microstructures were characterized mainly using scanning electron microscope (SEM; VEGAII, TESCAN) with energy dispersive spectrum (EDX). The sample preparation was reported in brief: samples were ground with water and ethanol down to a grinding size of 1500, polished with a lubricant containing 5 μm diamond particles followed by a lubricant containing 1 μm diamond particles. They were etched with a solution of 90 ml ethanol, 10 ml distilled water, 5 ml acetic acid and 5.5 g picric acid. X-ray diffraction (XRD) analysis was carried out on the polished samples of extruded CPP_p/ZK60A composites using an RIGAKU D/MAX-2400 diffractometer. The samples were exposed to Cu K_α radiation (λ = 1.5406 Å) with a step size of 0.02°.

Mechanical properties including compression and tensile tests were carried out at room temperature using an INSTRON 1195 universal testing machine. Samples

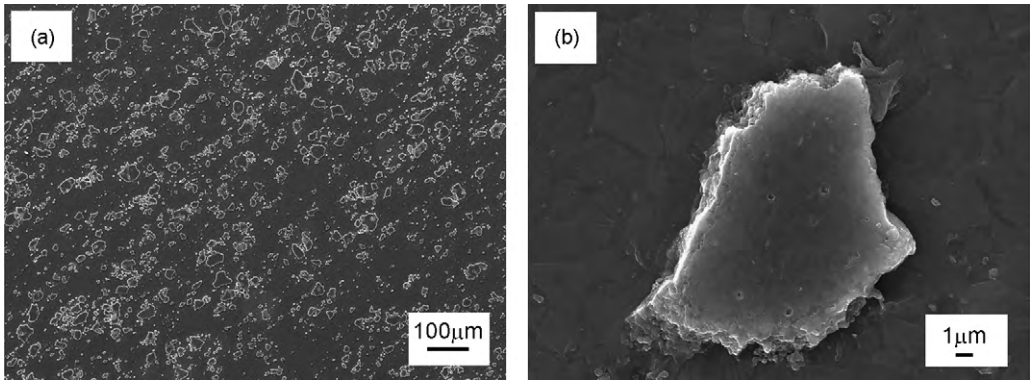

Fig. 1. SEM photograph of the $20CPP_p$/ZK60A composite: (a) low magnification which reveals the shape, average diameter and distribution of CPP particulates in ZK60A matrix and (b) high magnification which shows the good interfacial bonding between CPP and ZK60A.

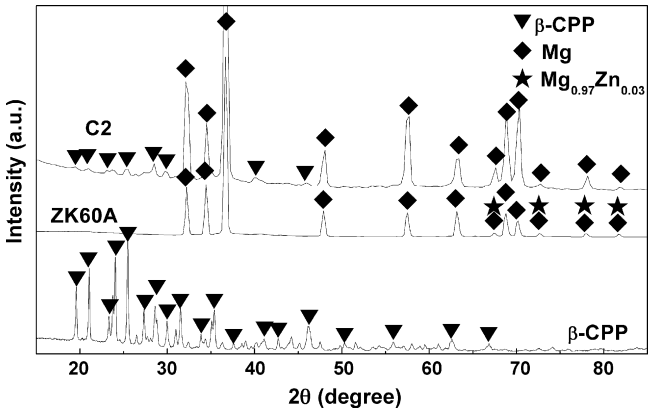

Fig. 2. XRD spectra of the CPP powders, ZK60A powders and $20CPP_p$/ZK60A composite in as-extruded state.

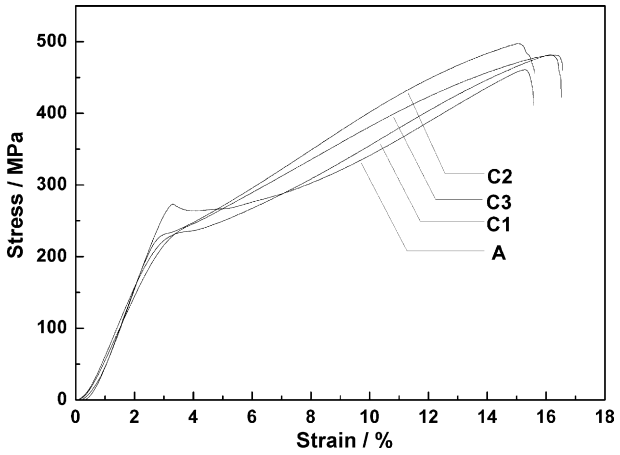

Fig. 3. The compressive stress–strain curves of the as-extruded ZK60A magnesium alloy and CPP_p/ZK60A composites.

were machined from the extruded rod. All tests were carried out in triplicates. For compression tests, cylindrical specimens of 6 mm in diameter and 10 mm in length were used. The tensile specimens with a gauge diameter of 5 mm and a gauge length of 25 mm were machined parallel to the extrusion direction.

Cylindrical samples for the immersion tests of 7 mm in diameter and 4 mm in length were cut from the extruded bar directly. All flat surfaces of samples were ground with SiC emery papers of up to 1500 grit and ultrasonically cleaned in alcohol for 5 min. The sample weight was measured before the immersion by a balance with accuracy of 0.1 mg. All the corrosion tests were carried out in simulated body fluids (SBF) with the following composition with a pH value of 7.4: NaCl (8.8385 g/l), $NaHCO_3$ (0.3905 g/l), KCl (0.2475 g/l), $K_2HPO_4{\cdot}3H_2O$ (0.2541 g/l), $MgCl_2{\cdot}6H_2O$ (0.3421 g/l), $CaCl_2$(0.3212 g/l), Na_2SO_4(0.0792 g/l), Tris (6.118 g/l) and

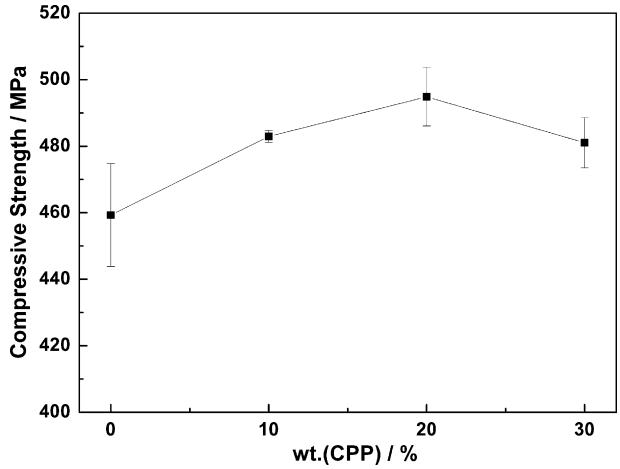

Fig. 4. The compressive strength of the as-extruded ZK60A magnesium alloy and CPP_p/ZK60A composites with the different CPP content.

HCl (pH modulation). The samples were immersed in 50 ml SBF solution at 37 ± 1 °C for up to 240 h. The immersion solution was refreshed every 48 h. Afterwards, the samples were ultrasonically washed with ethanol and dried. The weight measurements after immersion were carried out using chromic acid in order to remove the corrosion products. The change in the mass per surface area was calculated.

The electrochemical measurements were performed in SBF solution at 37 ± 1 °C. The cylindrical specimens were 7 mm in diameter and 4 mm in height. Samples were embedded into epoxy resin with only one flat surface (perpendicular to the extrusion direction) exposed for the testing. The working surface was ground with SiC emery papers of up to 1500 grit, and finely polished with a lubricant containing 5 μm diamond particles following 1 μm diamond particles, then ultrasonically cleaned in alcohol for 5 min. Electrochemical tests were carried out in a beaker containing 1000 ml SBF solution using a standard three electrode set-up, with a saturated calomel as a reference, a graphite electrode as a counter and the sample as the working electrode. In the potentiodynamic polarization tests, the working electrode was first immersed in SBF solution for 30 min and record the free corrosion potential. Then the polarization curve was measured at a scanning rate of 0.5 mV/s. The scan potential was set from −2.4 to 0 V. From the polarization curve the corrosion rate was determined using the Tafel slope.

3. Results

SEM micrograph in Fig. 1(a) shows the longitudinal microstructure of the $20CPP_p$/ZK60A composite which reveals the uniform distribution of CPP particulates and the absence of any distinct micrometer voids. The shape of the reinforcement is irregular and its average diameter is about 10 μm. As shown in high magnification (Fig. 1(b)), the interface of the matrix and reinforcement indicates good interfacial bonding between CPP and ZK60A in **C2** composite.

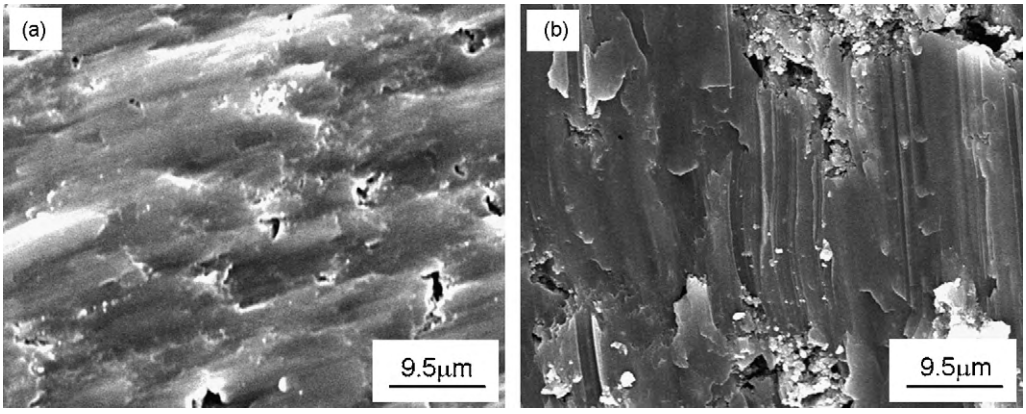

Fig. 5. SEM micrograph of the compressive fracture surfaces of the: (a) **A** alloy and (b) **C2** composite.

Fig. 2 shows XRD patterns of the CPP powder, ZK60A powder and the **C2** composite in as-extruded state. The CPP diffraction pattern shows the reflections of β-CPP with strong lines in the range of $2\theta = 15–40^{\circ}$. In XRD analysis, all the peaks in ZK60A powders were indexed as arising from the α-Mg phase and the second phase of $Mg_{0.97}Zn_{0.03}$. The diffraction pattern of the extruded 20CPP$_p$/ZK60A composite (Fig. 2) exhibited a little amount of CPP as well as a large amount of hcp-Mg reflections. By analyzing the XRD result of the composite, it indicated that there were no other detective phases from the reaction between the matrix and the CPP.

The compressive stress–strain curves of the as-extruded ZK60A magnesium alloy and the CPP$_p$/ZK60A composites are shown in Fig. 3. The compressive strength of the composites with different CPP content is shown in Fig. 4. Compared to ZK60A alloy, the composites with a mass of 10%, 20% and 30% CPP ceramic particulates have higher compressive strength, with the maximum obtained for **C2** composite (495 MPa). The fracture surfaces of the samples are shown in Fig. 5. For the alloy ZK60A (Fig. 5(a)), a planar and smooth fracture, interspersed with some shallow ridges and cleavage-like features can be seen. Moreover, cracks and voids were observed. All the composites show similar fracture. From Fig. 5(b) it can be seen that the large particles were crushed at the fracture of **C2** composite. And micropores were formed near the relatively small crushed particles. The matrix of the composites showed no voids and cracks comparing with the ZK60A alloy.

The ultimate strength and yield strength of the composites both decrease with the addition of CPP, as shown in Fig. 6. The elastic modulus (E) increased when the content of CPP was increased from 0% to 20% and then decreased. Fig. 7 shows typical SEM micrographs of tensile fracture for the **A** alloy and the **C2** composite. The fracture surface of ZK60A (Fig. 7(a)) reveals non-uniform ductile dimples indicating a ductile mode of fracture. For **C2** composite, matrix deformation, interfacial detachment and particulate fracture coupled with microscopic cracks were observed at the fracture surface (Fig. 7(b)–(d)).

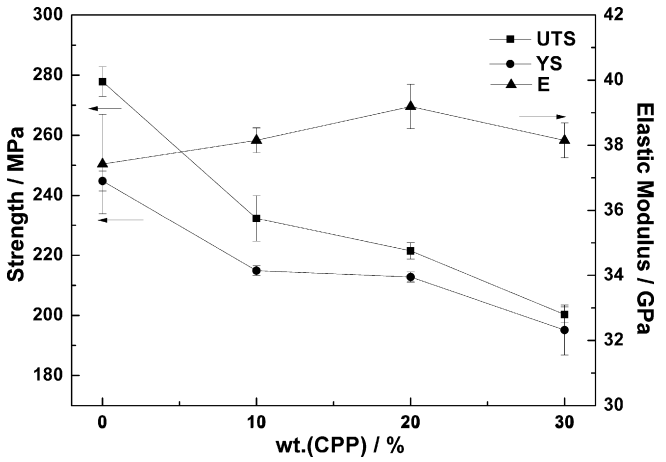

Fig. 6. The tensile ultimate strength (UTS), yield strength (YS) and elastic modulus (E) of the samples with the different CPP content.

The degradation behavior of ZK60A alloy and CPP$_p$/ZK60A composites was investigated by SBF immersion test. Immediately upon immersion, some bubbles began to appear on the surface for all the samples. Moreover, the surface of the samples changed to dark. After a few hours, the detached corrosion products were observed on the bottom of the beaker. Fig. 8 showed the weight loss of the samples in SBF solution during the preset immersion time. Composites show less weight loss in contrast to ZK60A at all test durations. Therefore we conclude that the composite structure was more corrosion resistant than the ZK60A alloys. During the immersion tests, the pH of the solution increased gradually as shown in Fig. 9. The

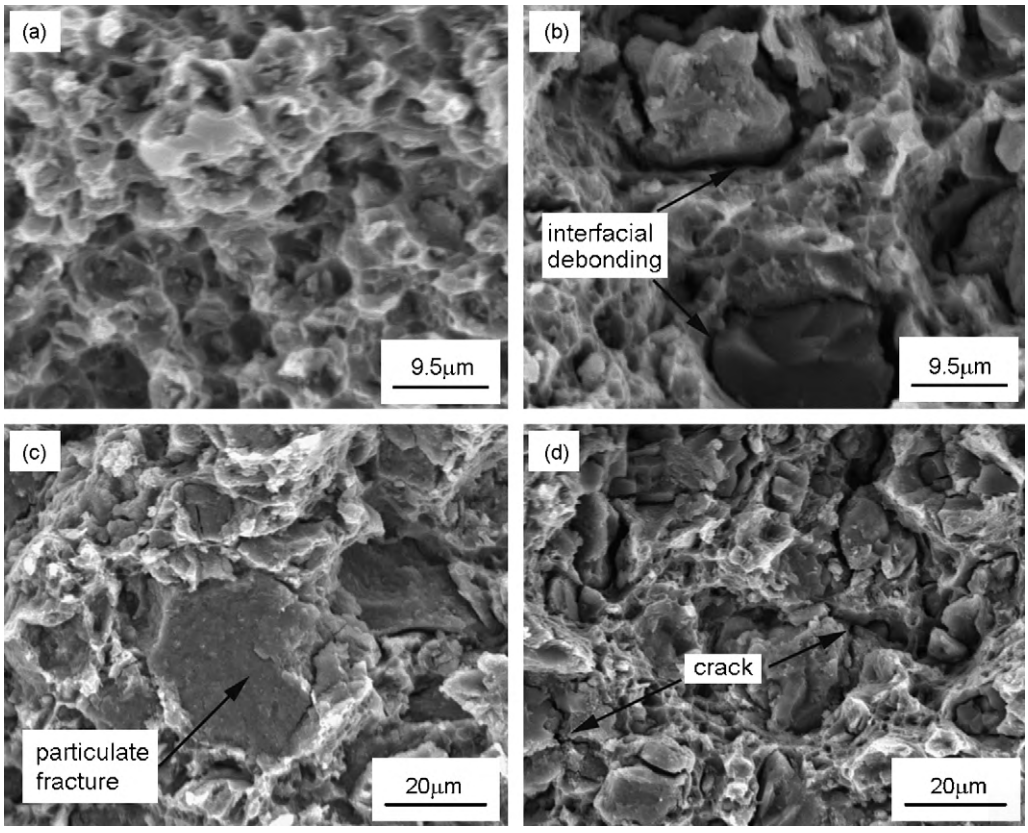

Fig. 7. SEM photographs of the tensile fracture surfaces of the as-extruded: (a) ZK60A and (b–d) **C2** composite with different failure mode which was labeled in graph.

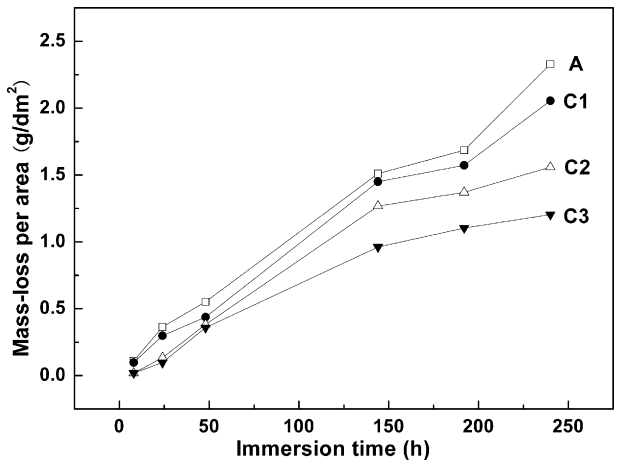

Fig. 8. Mass-loss per area of the ZK60A alloy and the composites with different CPP content immersed in SBF solution during the preset immersion time for up to 240 h.

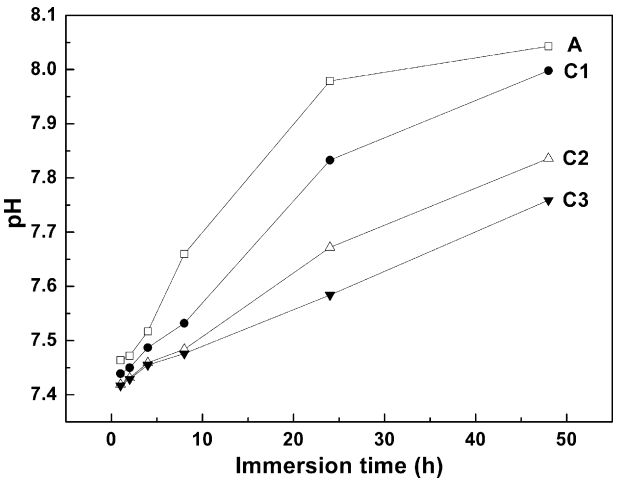

Fig. 9. The pH of the soak solution for different immersion time of the ZK60A alloy and the composites with different CPP content.

incorporation of CPP into magnesium alloys resulted in a significant decrease of the increasing amplitude to the pH value. The corrosion micrographs of the **A** and **C2** samples after immersed in SBF solution up to 240 h without removing the corrosion products was shown in Fig. 10. These corrosion samples showed localizing corrosion attack manifested as pitting corrosion. The product layer of the **A** sample revealed mud-cake type cracking phenomenon due to drying of the scale, which was rougher than that of the **C2** sample. The morphology of the precipitates of the **A** and **C2** samples after immersing up to 240 h was shown in Fig. 10(b) and (d). The precipitate of the **A** sample was sphere-shaped or nearly sphere-shaped with a size less than 100 nm in uniform distribution. However, the configuration of the precipitate of the **C2** sample was floriated. Higher magnification showed that it was the assembly of nanospheres to slices and further piled up to flower-shaped. The EDX results of the precipitates of the **A** and **C2** samples are shown in Fig. 11. The surface products of the **A** and **C2** samples are mainly composed of magnesium, calcium, phosphate and oxygen. However, the contents of calcium and phosphate in the **C2** sample are higher than those in **A** sample. Quantitative analysis (Table 2) indicates that the Ca/P atomic ratio of the surface products of the **C2** samples is 1.36, which is close to that of hydroxyapatite (1.67).

Fig. 12 shows typical electrochemical polarization curves for the ZK60A alloy and the composites in SBF in 37 °C. The data of

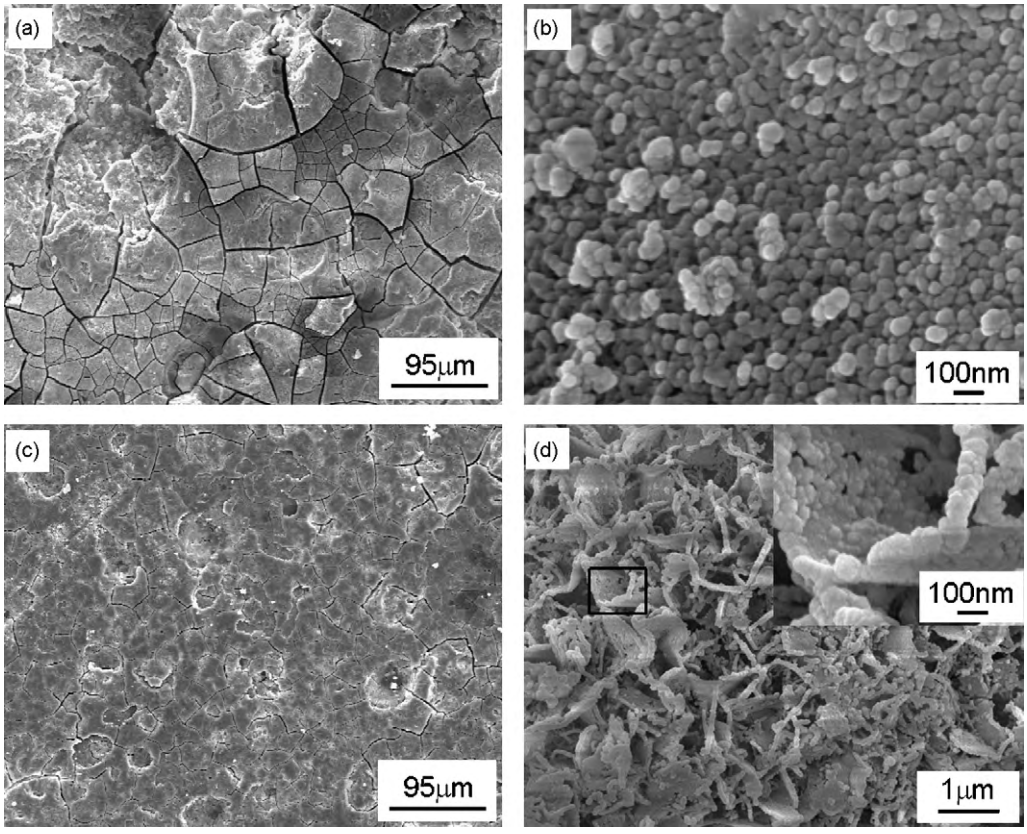

Fig. 10. The SEM micrograph of the: (a) **A** sample in low magnification; (b) **A** sample in high magnification; (c) **C2** sample in low magnification; and (d) **C2** sample in high magnification in which the inset is local magnification for the rectangular frame after immersed in SBF solution up to 240 h without removing the corrosion products.

Table 2
Representative composition of the precipitates of the **A** and **C2** samples.

Sample	Content (%)	O	Mg	P	Ca	Zn	Total
A	wt.	36.94	45.31	4.46	3.26	10.02	100.00
	at.	50.73	40.95	3.16	1.79	3.37	100.00
C2	wt.	44.32	5.69	18.09	31.90	–	100.00
	at.	63.19	5.34	13.32	18.15	–	100.00

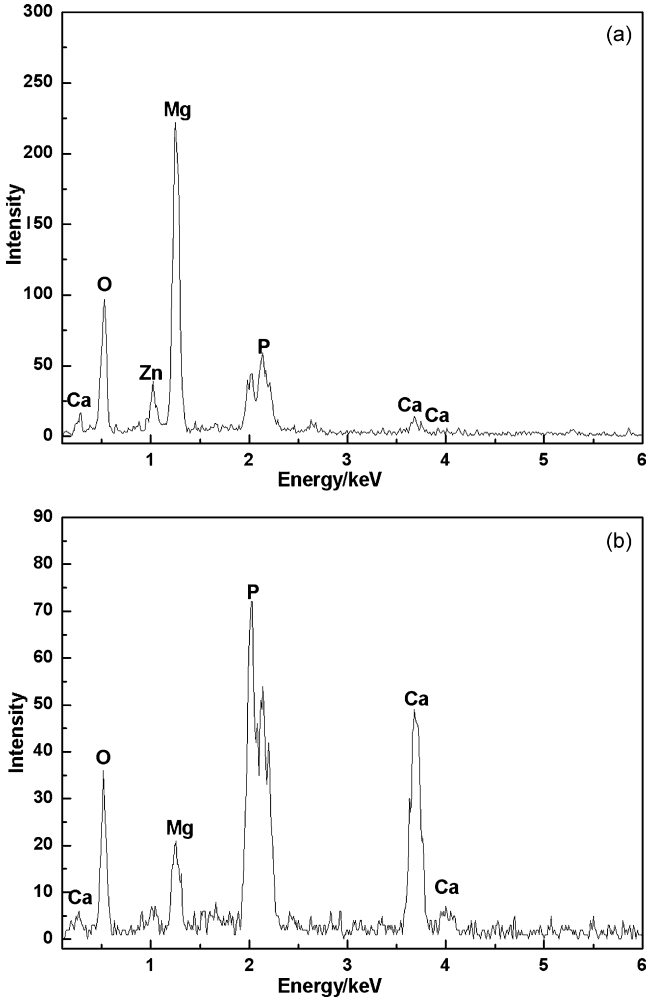

Fig. 11. The EDX of the precipitates of the: (a) **A** sample and (b) **C2** sample after immersed in SBF solution up to 240 h which are correspond to Fig. 10(b) and (d), respectively.

the corrosion potential E_{corr} and the corrosion current density i_{corr} extracted from Fig. 12 are shown in Table 3. The E_{corr} was ennobled by about 40 mV due to calcium polyphosphate addition to magnesium alloy for the **C2** sample. The corrosion current density of the samples, given in Table 3, suggested that CPP addition substantially reduced the i_{corr} of magnesium alloy.

The micro-corrosion morphologies of the **A** and **C2** samples after the polarization tests in simulated body fluid are shown in Fig. 13. There are many deep pits in the corroded areas on the two samples and the corrosion was localized. The corroded surface exhibited a

Table 3
Electrochemical parameters of the **A**, **C1**, **C2** and **C3** samples.

Parameters	A	C1	C2	C3
E_{corr} (V SCE)	−1.60	−1.58	−1.56	−1.52
i_{corr} (μA/cm^2)	0.116	0.092	0.088	0.077

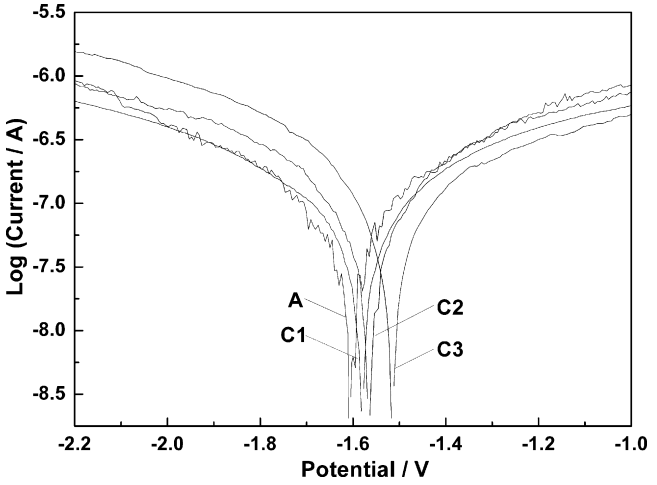

Fig. 12. Polarization curves of the **A**, **C1**, **C2** and **C3** samples in simulated body fluid in 37 °C.

porous morphology. Many cracks can also be observed. In comparison with **A** sample, less corrosion attack was found on the surface of the **C2** sample. For some regions severely attacked, the **A** and **C2** samples broke off and the surface became coarse (Fig. 13(b) and (e)). As shown in Fig. 13(c) and (f), the corrosion layer was formed, which will impeded corrosion to some extent. The surface layer morphologies of the **A** and **C2** samples were different. The **A** sample had a lubricous surface layer, while the **C2** sample had an alveolate layer.

4. Discussion

Metal magnesium has been developed as a potential implant material due to its good biocompatibility. So far, magnesium alloys as biodegradable metal stents have been in clinical trials. In this paper, we have prepared magnesium alloy-based MMCs using magnesium alloy ZK60A as matrix and CPP particles as reinforcement which had appropriate mechanical and corrosive properties. The results indicated that CPP_p/ZK60A could be used as a candidate for current implant materials in orthopedic and trauma surgery.

The microstructural analyses of the 20CPP_p/ZK60A composites show a homogeneous distribution of CPP particles within the ZK60A magnesium matrix, which can result in consistent mechanical properties and a homogenous corrosion process. Poddar et al. [24] synthesized AZ91D based composites reinforced with 15 vol.% SiC particulates whose average particle size was 15 μm by stir casting technique. The results showed that the agglomeration of SiC particles occurred in some areas which may be due to the fine particle size. Particles of small sizes are prone to clustering, and also, the growth of primary α-Mg grains pushes the particles towards grain boundaries for stir casting technique. Hence, the powder metallurgy method used in this paper was more suitable for preparing uniform MMCs compared with stir casting technique. XRD studies revealed that there was no other detectable reactive phase in the samples. The product of the interfacial reactions may have weakened the interfacial bonding between CPP and matrix [25]. It was

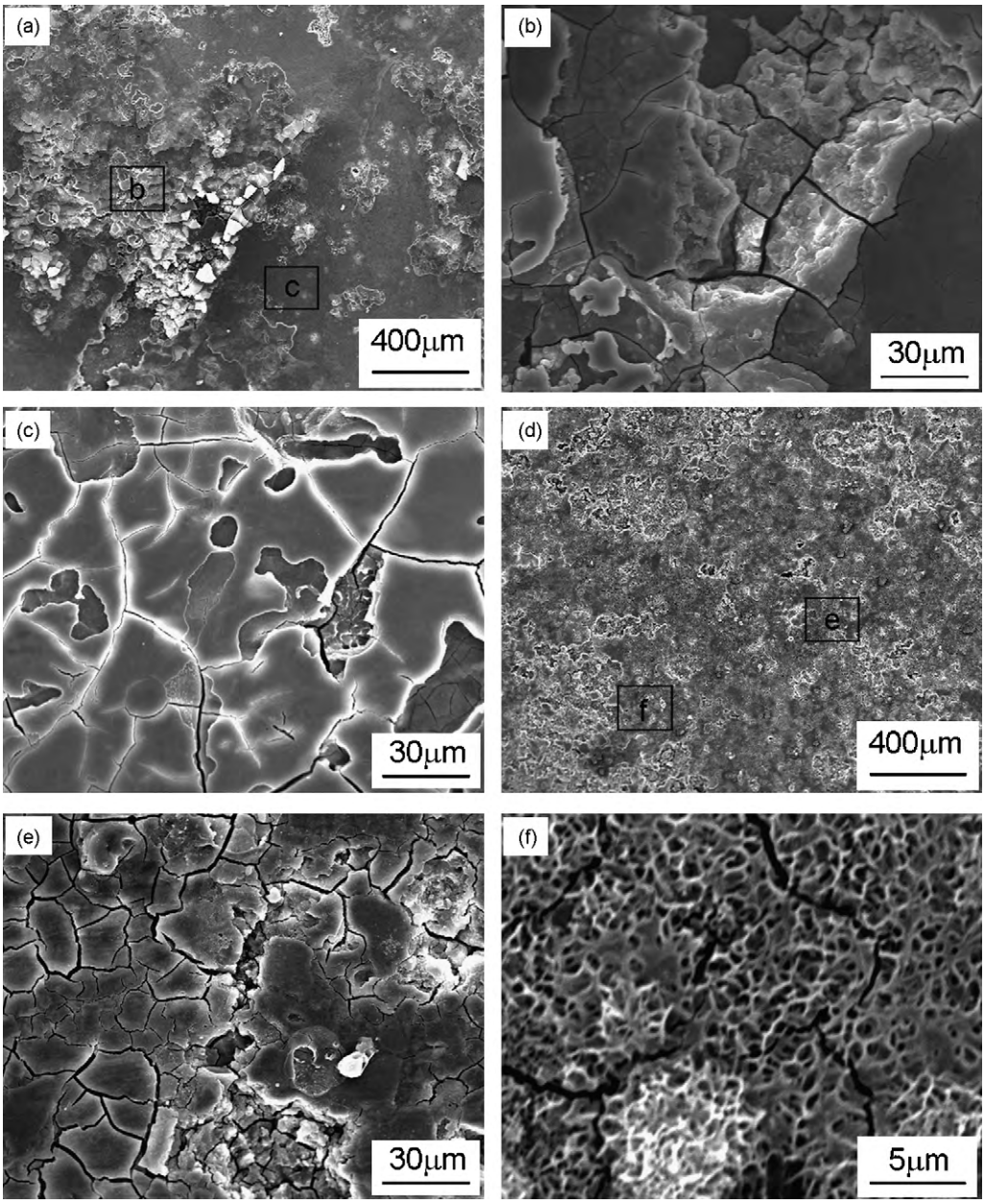

Fig. 13. SEM micrograph of the: (a–c) **A** sample and (d–f) **C2** sample after the potentiodynamic polarization tests in simulated body fluid in 37 °C.

favorable to enhance the interfacial properties when there was no reactive phase. Furthermore, the interface morphology indicated the intact interfacial bonding between CPP and ZK60A in the MMCs.

The results of compressive tests revealed improvement in ultimate compressive strength of the composites compared with the as-extruded magnesium alloy, which was primarily attributed to the effective transfer of applied compressive load to the uniformly distributed CPP particulates. Moreover, a large number of reinforcing CPP and the numerous boundaries act as obstacles to the dislocation movement and end up with dislocation pile ups. The strain mismatch between the matrix and the reinforcement usually generates a higher density of dislocation in the matrix around the reinforcement, thus strengthening the material. Fracture surface of magnesium alloy ZK60A was rugged and some voids can be seen (Fig. 5(a)). Failure in form of CPP particle fracture was observed distinctly as a dominant failure mode of the composites (Fig. 5(b)) in compressive tests. The presence of hard, intrinsically brittle and elastically deforming CPP_p in a relative soft and ductile magnesium alloy matrix results in limited flow stress and constrained mechanical deformation which facilitates the concentration of stress at the particulates [26].

Comparing to matrix ZK60A alloy, the composites exhibit an overall lower 0.2% yield strength and tensile strength. Generally, the basic mechanism of composite deformation is the load transfer from the soft matrix to the hard reinforcement. Due to the much higher strength of the secondary hard phases, the relatively soft matrix is protected. A good bonding between the matrix and the reinforced particles gives rise to better load transfer and the improved properties. In a composite material, a tensile load leads to high tensile stresses at the interface. This may give rise to detachment at the interface or breaking of particles. A poorly bonded interface induces detachment. Whereas, a good bonding leads to failure of ceramic particles. The fracture surface of the **A** alloy (Fig. 7(a)) revealed a wide size range of ductile dimples. In the case of **C2** specimen, evidence of areas of reasonable plastic deformation was observed and this indicated strain accumulation at the

CPP–matrix interface. The interfacial detachment and CPP particle fracture were observed in SEM (Fig. 7(b) and (c)). Such localized damage occurs under high stress condition. The coalescence of the local damage at even higher strain levels then leads to the final fracture of the composite materials [24]. Crack forms and propagates in the reinforcement-free areas in the matrix (Fig. 7(d)). In this case, the matrix played a more important role in determining the deformation and fracture behavior of the composites. The prepared $20CPP_p$/ZK60A had a tensile yield strength of 212.77 MPa, which agrees with the characteristics of natural bone [2]. The mechanical characteristics indicated that MMCs were suitable for the degradable implants in load bearing applications.

For magnesium alloys to be used as biodegradable implant materials, their degradation rates should not exceed the rate of healing of the affected tissue, and also the degradation products should not be more than the body's acceptable absorption level. In fact, although Mg is compatible with human body and the direct corrosion product Mg^{2+} can be tolerated, the corrosion by-products of magnesium, such as hydrogen gas and hydroxides, are not physiologically favorable [27]. Normally, the measurement of corrosion rate of Mg alloys includes measuring the weight loss and the corrosion current density. The **C2** composite shows a lower weight loss while the ZK60A alloy shows a higher weight loss at all test durations. So the composite **C2** was more corrosion resistant than the ZK60A alloy. Furthermore, the pH of the solution immersed with the **C2** sample was lower than that immersed with the **A** sample. Thus, the CPP addition can stabilize the pH value at some degree. As it is known, the increase of the pH values in solutions mainly results from the formation of corrosion product $Mg(OH)_2$. The microstructural observation showed that the **C2** composite was corroded more uniformly than the **A** alloy in the simulated body fluid. And the **A** sample was more prone to pitting corrosion. The resistance against pitting corrosion depends on metallurgical factors (impurities, processing), the formation of surface films, the concentration of pitting anion, as well as pH value of the corrosive solution [28]. The breakdown of the protective layer was responsible for the observed local corrosion, which occurred randomly during the whole test period. Hence, the surface films formed on the **C2** sample can protect it from corrosion effectively. It was also found that the region near CPP was corroded more seriously, which may caused by its cathodic nature (i.e., noble with respect to matrix) and the distance effect of galvanic corrosion. The precipitate on the **A** sample after immersion was sphere-shaped or nearly sphere-shaped and that of **C2** was floriated. The surface products of the **A** sample were inferred as mainly magnesium hydroxide or magnesium oxygen by EDX (Fig. 11(a)). The corrosion product $Mg(OH)_2$ is not stable in aqueous solutions, especially in chloride containing environments [29]. It should be noted that the alloying elements Al and Zn tend to have a stabilizing effect on the protective film formed on the Mg alloy. On the other hand, the precipitation products of the **C2** sample are mainly composed of calcium, phosphate and oxygen (Fig. 11(b)). The Ca/P atomic ratio of the surface products of the **C2** sample is 1.36, which is close to that of hydroxyapatite (1.67). Witte et al. [17] reported calcium phosphate (hydroxyapatite) formation on the surface of magnesium-based composite HA/AZ91D in their *in vitro* studies. Corrosion tests revealed that HA particles stabilized the corrosion rate and exhibited more uniform corrosion attack in artificial seawater and cell solutions. It was also reported that calcium-ion implantation in titanium accelerated the precipitation of calcium phosphate. Kannan and Raman [15] suggested that the high amount of calcium present in AZ91Ca alloy have enhanced the formation of calcium phosphate on the surface and consequently improved the corrosion resistance. *In vitro* corrosion studies showed that calcium addition improved the general and pitting corrosion resistance of magnesium alloy significantly. Li et al. [9] showed that Ca–P based apatite with molar ratio of 1.858 was detected after the alkali-heat-treated magnesium samples had been soaked in SBF for 14 days. Therefore, it can be inferred that amorphous calcium phosphate or magnesium calcium apatite ($((Ca_{1-x}Mg_x)_{10}(PO_4)_6(OH)_2$) precipitation can form on the surface of magnesium alloys when soaked in the SBF. If osteo-conductive apatite coating can be successfully deposited on magnesium alloy composites in a biological environment, such coating will also form *in vivo*, which thus benefiting biomedical applications of the composites. Kim et al. [30] indicated corrosion rate can be controlled by adjusting the Mg_2Ca phase distribution in the Mg–Ca alloy system. The formation of a galvanic cell between the Mg anode and Mg_2Ca cathode accelerated corrosion rate.

The electrochemical corrosion tests show the same tendency as the immersion results. The corrosion potential was ennobled by 40 mV from −1.60 V to −1.56 V due to calcium polyphosphate addition to magnesium alloy for the **C2** sample. The corrosion current density of the samples suggested that CPP addition substantially reduced the i_{corr} of magnesium alloy from 0.116 μA/cm^2 to 0.088 μA/cm^2 for the **C2** sample. Tafel slopes were similar for the two materials, indicating similar reaction mechanism even with the incorporation of CPP. The SEM micrographs showed that the **A** alloy exhibited large pits, whereas such pit morphology was not evident in the **C2** composite. The corrosion film was formed on both **A** and **C2** samples, which impeded corrosion to some extent. The polarization results of Kim et al. [30] showed that the corrosion current of AZ91Ca alloy was almost four times lower than that of AZ91 alloy. It indicated that addition of calcium can reduce corrosive rate. NunezLopez et al. [31] indicated that incorporation of silicon carbide particles did not result in significant microgalvanic corrosion for magnesium-based MMCs. Tiwari et al. [32] suggested that the basic corrosion mechanism was not affected by the incorporation of SiC in Mg. There are some other methods to improve the corrosive properties of magnesium and its alloys. Li et al. [9] suggested that the alkali-heat-treated magnesium samples showed an improved corrosion resistance in SBF solutions as compared to untreated magnesium samples. The present study of Wang et al. [33] had shown that the biodegradation rate of alloy AZ31 in Hank's solution can be significantly reduced due to grain refinement by mechanical processing. Liu et al. [34] indicated that changes in the microstructure of the aged die-cast AZ63 Mg alloy had a great influence on the corrosion performance in the simulated body fluid.

The prepared composites can be used as biodegradable bone implant materials since CPP and ZK60A are all biodegradable and biocompatible materials. As compared with Mg–Ca alloys, the $20CPP_p$/ZK60A composed of a larger amount of Ca element, and element P also exists in the composites. The existence of Ca and P induced the formation of hydroxyapatite when MMCs were exposed in SBF solutions. Witte et al. [28] concluded that the corrosion rates achieved from *in vivo* tests were about four orders of magnitude smaller than those achieved from *in vitro* tests. Further investigation on *in vitro* cell tests and *in vivo* animal experiments will be carried out.

5. Conclusions

The CPP_p/ZK60A magnesium-matrix composites were fabricated by powder metallurgy route, which were extruded at 380 °C with an extrusion ratio of 16:1. The mechanical and corrosive properties of the composites were investigated. The main results of the work can be summarized as follows. The composite prepared by present processing has uniform distribution of CPP particulates in the matrix and the closely bonded CPP–magnesium alloy interface. The maximum compressive strength was obtained from composites of 20 wt.% CPP which is about 494.88 MPa, 35 MPa higher than that of ZK60A. Failure in the form of CPP fracture was observed

distinctly as a dominant failure mode of the composites in compressive tests, which may be attributed to the effective transfer of applied compressive load from the ductile matrix to the uniformly distributed CPP particulates. The ultimate and the yield strengths of the composites were reduced by CPP addition in tensile test. The ZK60A alloy exhibited ductile fracture, while the composite with 20 wt.% CPP showed matrix deformation, interfacial detachment and particulate breakage coupled with microscopic cracks at the tensile fracture. The addition of CPP particles improved corrosion resistance of the composites, and accelerated hydroxyapatite precipitation from the simulated body fluid. In summary, the studies show that the CPP_p/ZK60A magnesium-matrix composite has suitable mechanical and corrosive properties, and could be used as a degradable material for implant applications.

Acknowledgements

The authors gratefully acknowledge for the help and encouragement of Prof. Donglang Chai and excellent technical assistance of M. Xinjie Zhang, M. Cunhui Li and M. Ge Tian during the present work.

References

[1] R.V. Marrey, R. Burgermeister, R.B. Grishaber, R.O. Ritchie, Biomaterials 27 (2006) 1988–2000.
[2] M.P. Staiger, A.M. Pietak, J. Huadmai, G. Dias, Biomaterials 27 (2006) 1728–1734.
[3] J.Y. Wang, B.H. Wicklund, R.B. Gustilo, D.T. Tsukayama, Biomaterials 17 (1996) 2233–2240.
[4] H. Zreiqat, C.R. Howlett, A. Zannettino, P. Evans, G. Schulze-Tanzil, C. Knabe, M. Shakibaei, J. Biomed. Mater. Res. 62 (2002) 175–184.
[5] Y. Yamasaki, Y. Yoshida, M. Okazaki, A. Shimazu, T. Kubo, Y. Akagawa, T. Uchida, Biomaterials 24 (2003) 4913–4920.
[6] F. Witte, V. Kaese, H. Haferkamp, E. Switzer, A. Meyer-Lindenberg, C.J. Wirth, H. Windhagen, Biomaterials 26 (2005) 3557–3563.
[7] F. Witte, H. Ulrich, M. Rudert, E. Willbold, J. Biomed. Mater. Res. Part A 81A (2007) 748–756.
[8] G.L. Song, Corros. Sci. 49 (2007) 1696–1701.
[9] L.C. Li, J.C. Gao, Y. Wang, Surf. Coat. Technol. 185 (2004) 92–98.
[10] Y.W. Song, D.Y. Shan, E.H. Han, Mater. Lett. 62 (2008) 3276–3279.
[11] K.Y. Chiu, M.H. Wong, F.T. Cheng, H.C. Man, Surf. Coat. Technol. 202 (2007) 590–598.
[12] C.L. Liu, Y.C. Xin, X.B. Tian, P.K. Chu, Thin Solid Films 516 (2007) 422–427.
[13] C.G. Liu, Y.C. Xin, X.B. Tian, J. Zhao, P.K. Chu, J. Vac. Sci. Technol. A 25 (2007) 334–339.
[14] Z.J. Li, X.N. Gu, S.Q. Lou, Y.F. Zheng, Biomaterials 29 (2008) 1329–1344.
[15] M.B. Kannan, R.K.S. Raman, Biomaterials 29 (2008) 2306–2314.
[16] L.P. Xu, G.N. Yu, E. Zhang, F. Pan, K. Yang, J. Biomed. Mater. Res. Part A 83A (2007) 703–711.
[17] F. Witte, F. Feyerabend, P. Maier, J. Fischer, M. Stormer, C. Blawert, W. Dietzel, N. Hort, Biomaterials 28 (2007) 2163–2174.
[18] S. Landgraeber, M. von Knoch, F. Loer, A. Wegner, M. Tsokos, B. Hussmann, M. Totsch, Biomaterials 29 (2008) 3444–3450.
[19] L.V. Branzoi, M. Iordoc, M. Codescu, Surf. Interface Anal. 40 (2008) 167–173.
[20] K. Qiu, X.J. Zhao, C.X. Wan, C.S. Zhao, Y.W. Chen, Biomaterials 27 (2006) 1277–1286.
[21] N.L. Porter, R.M. Pilliar, M.D. Grynpas, J. Biomed. Mater. Res. 56 (2001) 504–515.
[22] M.D. Grynpas, R.M. Pilliar, R.A. Kandel, R. Renlund, M. Filiaggi, M. Dumitriu, Biomaterials 23 (2002) 2063–2070.
[23] R.M. Pilliar, M.J. Filiaggi, J.D. Wells, M.D. Grynpas, R.A. Kandel, Biomaterials 22 (2001) 963–972.
[24] P. Poddar, V.C. Srivastava, P.K. De, K.L. Sahoo, Mater. Sci. Eng. A: Struct. Mater. Prop. Microstruct. Process 460 (2007) 357–364.
[25] B.W. Chua, L. Lu, M.O. Lai, Compos. Struct. 47 (1999) 595–601.
[26] J.Q. Li, L. Wang, H.W. Cheng, H.F. Zhang, Z.Q. Hu, H.N. Cai, Mater. Sci. Eng. A: Struct. Mater. Prop. Microstruct. Process 474 (2008) 24–29.
[27] G.L. Song, S.Z. Song, Adv. Eng. Mater. 9 (2007) 298–302.
[28] F. Witte, J. Fischer, J. Nellesen, H.A. Crostack, V. Kaese, A. Pisch, F. Beckmann, H. Windhagen, Biomaterials 27 (2006) 1013–1018.
[29] G.L. Song, Adv. Eng. Mater. 7 (2005) 563–586.
[30] W.C. Kim, J.G. Kim, J.Y. Lee, H.K. Seok, Mater. Lett. 62 (2008) 4146–4148.
[31] C.A. NunezLopez, H. Habazaki, P. Skeldon, G.E. Thompson, H. Karimzadeh, P. Lyons, T.E. Wilks, Corros. Sci. 38 (1996) 1721–1729.
[32] S. Tiwari, R. Balasubramaniam, M. Gupta, Corros. Sci. 49 (2007) 711–725.
[33] H. Wang, Y. Estrin, Z. Zuberova, Mater. Lett. 62 (2008) 2476–2479.
[34] C.L. Liu, Y.C. Xin, G.Y. Tang, P.K. Chu, Mater. Sci. Eng. A: Struct. Mater. Prop. Microstruct. Process 456 (2007) 350–357.